

It is seen that the two experimental values of Berkner, *et al.* are less than the corresponding OBK values, which fact suggests that the asymptotic energy region may not yet be reached. Of course, it is not known whether OBK cross sections are the asymptotic values of a correct theory, and at what energy the onset of the asymptotic value would occur. Little is also known how well electron capture from N_2 can be described in terms of N atoms⁸ (factor of 2) or how much the present OBK values would be altered by a recalculation with improved wave functions. In the author's

⁸ T. F. Tuan and E. Gerjuoy, *Phys. Rev.* **117**, 756 (1960).

opinion, it is very difficult to decide theoretically what the asymptotic cross section is for a target as complicated as N_2 .

An atomic system much more tractable to theoretical analysis is helium, and the energy range of the OBK calculations⁹ using the 6-parameter helium wave function have also been extended to 100 MeV. The OBK cross sections for capture from He, N, and O, described in this paper, can be obtained from the author.

Gratitude is expressed to Professor A. Dalgarno for informing the author of these measurements.

⁹ R. A. Mapleton, *Phys. Rev.* **130**, 1839 (1963).

Radiative Lifetime of the First $^2P_{3/2}$ State of Ionized Calcium and Magnesium by the Hanle Effect*

WINTHROP W. SMITH^{††} AND ALAN GALLAGHER

Joint Institute for Laboratory Astrophysics, § Boulder, Colorado

(Received 1 November 1965)

The lifetime of the Ca^+ $4^2P_{3/2}$ state and that of the Mg^+ $3^2P_{3/2}$ state have been measured by the Hanle-effect method with optical excitation from the ground states of the ions. The lifetimes are, respectively, $(6.72 \pm 0.20) \times 10^{-9}$ and $(3.67 \pm 0.18) \times 10^{-9}$ sec. The ions were produced by introducing traces of calcium or magnesium into an argon discharge. "Alignment" depolarization cross sections σ were obtained for the collisional depolarization of the following states of calcium and magnesium due to collisions with argon:

$$\begin{aligned}\sigma(Ca\ 4^1P_1\ \text{state}) &= (1.9 \pm 0.3) \times 10^{-14}\ \text{cm}^2; \\ \sigma(Ca^+\ 4^2P_{3/2}\ \text{state}) &= (1.4 \pm 0.2) \times 10^{-14}\ \text{cm}^2; \\ \sigma(Mg\ 3^1P_1\ \text{state}) &= (1.9 \pm 0.3) 10^{-14}\ \text{cm}^2; \\ \sigma(Mg^+\ 3^2P_{3/2}\ \text{state}) &= (1.3 \pm 0.25) \times 10^{-14}\ \text{cm}^2.\end{aligned}$$

The magnitudes of these cross sections are in accord with the theories of Byron and Foley and of Omont; we give a discussion of the extension of these theories to include ion-atom collisions.

I. INTRODUCTION

WE report here the application of the Hanle-effect technique to the measurement of lifetimes of excited states of ions. Ca^+ and Mg^+ were chosen, since their absolute oscillator strengths are of astrophysical importance and are useful for testing various theoretical methods of calculating oscillator strengths.¹ The Hanle effect has been known for many years as a technique for measuring lifetimes or transition probabilities for optical resonance lines in atoms.² The method has been

used frequently in recent years, primarily by the group at Columbia.³ This recent work has demonstrated the accuracy of the method for measuring atomic state lifetimes (a typical uncertainty is 3%), and it is an aim of the present paper to demonstrate that the method can be used to measure ionic state lifetimes with comparable accuracy. Although the results reported here are only for Group II ions, we think that the method should have wide application for precision determinations of transition probabilities of resonance lines of other ions.

Methods for measuring transition probabilities of atoms or ions may be divided into two classes: those which measure oscillator strengths directly and those which measure excited-state lifetimes. Typical of the first class are the methods of anomalous dispersion (the "hook" method),² emission from thermal arcs,⁴ and *and Excited Atoms* (Cambridge University Press, New York, 1961), Chap. V.

³ For a review of the theory and experimental techniques, see A. Lurio, R. L. deZafra, and R. J. Goshen, *Phys. Rev.* **134**, A1198 (1964), and references contained therein.

⁴ See, for example, C. H. Corliss and W. R. Bozman, *Natl. Bur. Std. (U. S.) Monograph* 53 (1962).

* Work was supported by the National Bureau of Standards and by the Advanced Research Projects Agency (Project DEFENDER), monitored by the U. S. Army Research Office-Durham, under Contract DA-31-124-ARO-D-139.

[†] Present address: Department of Physics, Columbia University, New York, New York.

[‡] National Academy of Sciences-National Research Council Postdoctoral Fellow assigned to National Bureau of Standards (1963-65).

[§] Of the University of Colorado and the National Bureau of Standards, Boulder, Colorado.

¹ See, for example, A. S. Douglas and R. H. Garstang, *Proc. Cambridge Phil. Soc.* **58**, 377 (1962).

² A. C. G. Mitchell and M. W. Zemansky, *Resonance Radiation*

absorption measurements.² All of these methods really measure the product of the density of atoms or ions and the oscillator strength. Since the density is often difficult to determine in the atomic case, and since the percent of ionization in the ion case adds further uncertainty, these methods are usually more reliable for relative oscillator strengths than for absolute oscillator strengths (this is particularly true for ions). The methods which measure excited state lifetimes, rather than oscillator strengths as such, do not require knowledge of the absolute density. The measured lifetimes do depend on the density through radiation trapping and collisional mechanisms, but in the limit of low density these perturbations become negligible.^{5,6} The lifetime measurements can be done in a great variety of ways, for example, by direct measurement of the exponential decay following a brief excitation pulse,⁷ by measurement of phase shifts between exciting (modulated) radiation or electron beam and emitted radiation,⁸ by natural linewidth determinations using optically or electronically excited double resonance,⁹ and by the Hanle effect. The possibility of using the Hanle effect for lifetime measurements with electron excitation rather than with optical excitation is apparent from the polarization measurements of Skinner and Appleyard.¹⁰ This has now been used for both atom and ion excited states.¹¹ The magnetic-resonance and Hanle-effect experiments on ions by electron excitation must overcome the difficulties of a small-percentage polarization in the excited state as well as the influence of the magnetic field on the electron beam. By using optical excitation from the ionic ground state, as reported here, the ion excited state is highly polarized; but one is restricted to studies of resonance lines in the ions.

The Hanle effect with optical excitation may be described¹² as the scattering of resonance radiation by the ions or atoms under study while they are subjected to a small and variable magnetic field. If the field at

the site of the ion is zero, it is possible to excite magnetic sublevels of the excited state coherently by absorption of a single photon with the appropriate polarization. When the magnetic field is turned on, the angular distribution of the scattered light then depends on the amount of overlap of the nearly degenerate levels of the excited state, which is determined by the ratio of the radiation width ($1/\tau$) to the Zeeman splitting. By measuring the change in scattered intensity at a particular angle with magnetic field, one can determine the radiation width ($1/\tau$) in terms of the Lande g factor of the excited state. It is important to note that the Hanle-effect technique does not require knowledge of the absolute intensity or the number of scatterers, although multiple-scattering narrowing (coherence narrowing) of the natural linewidth must be evaluated. (This is generally done by finding the limiting value of the lifetime as the density of scatterers is reduced toward zero.) The scattering cross section of an ion for its own resonance radiation is so large² that the low-multiple-scattering limit is reached at pressures of the order of 10^{-5} Torr or less. Consequently, the data are taken at ion densities below $10^{11}/\text{cc}$, where ion-ion collisional or Stark perturbations have a negligible influence on the excited state lifetimes.

In the present experiment the ions are produced by running a discharge in a foreign gas. The resulting collisional perturbations of the natural lifetime have been evaluated by the method described in Sec. IV, B and C. An additional complication is the slight magnetic-field dependence of the number of ions produced in the discharge; this field dependence has been evaluated by the method described in Sec. IVA.

II. THEORY

A complete description of the Hanle effect (and of resonance fluorescence by nearly degenerate levels in general) is contained in a formula first derived by Breit¹³ and later rederived by Franken and others^{12,14}; we will use this formula to interpret the experiments.

The first few energy levels of Ca^+ and Mg^+ are shown in Fig. 1. Ninety-nine percent of naturally occurring calcium consists of zero-nuclear-spin isotopes, while 90% of natural magnesium consists of zero-nuclear-spin isotopes and 10% is Mg^{25} with nuclear spin $I = \frac{5}{2}$. Thus the Breit formula can be evaluated for Ca^+ without considering hfs, whereas the $3^2P_{3/2}(F, m_F)$ states of Mg^{25} have g_F values differing from g_J , and they will produce Hanle-effect linewidths differing from that of the even isotopes. However, it is easily shown from the Breit formula that the effect of the odd isotope on the measured width in Mg^+ is a maximum of 0.3%, even with the assumption of equal lamp intensity exciting all isotopes. Both Ca^+ and Mg^+ will therefore

⁵ J. P. Barrat, *J. Phys. Radium* **20**, 633 (1959).

⁶ A. Lurio and R. Novick, *Phys. Rev.* **134**, A608 (1964).

⁷ This technique has been used on atoms by S. Heron, R. W. P. McWhirter, and E. H. Roderick, *Proc. Roy. Soc. (London)* **A234**, 565 (1956) and by W. R. Bennett, Jr., in *Advances in Quantum Electronics*, edited by J. Singer (Columbia University Press, New York, 1961).

⁸ For example, W. Demtröder, *Z. Physik.* **166**, 42 (1962), who used the phase-shift method in atoms; modulated electron beams have been used to measure lifetimes of excited states of molecular ions by G. M. Lawrence, *J. Quant. Spectry. Radiative Transfer* **5**, 359 (1965).

⁹ The original optical double resonance experiment of Brossel and Bitter, *Phys. Rev.* **86**, 308, (1952), has been applied to atomic excited states which cannot be reached optically using excitation by electron beams by J. C. Pebay-Peyroula, *J. Phys. Radium (Paris)* **20**, 669, 721 (1959) and to ion state lifetimes by E. Geneux and B. Wanders-Vincenz, *Phys. Rev. Letters* **3**, 422 (1959).

¹⁰ H. W. B. Skinner and E. T. S. Appleyard, *Proc. Roy. Soc. (London)* **A117**, 224 (1928).

¹¹ J. C. Pebay-Peyroula *et al.*, *Compt. Rend.* **256**, 5088 (1963) and **257**, 3130 (1963). For ion excited state measurements see W. Kahan, T. Lucatorro, and R. Novick, *Bull. Am. Phys. Soc.* **9**, 451 (1964).

¹² See P. Franken, *Phys. Rev.* **121**, 508 (1961).

¹³ G. Breit, *Rev. Mod. Phys.* **5**, 91 (1933).

¹⁴ M. E. Rose and R. L. Carovillano, *Phys. Rev.* **122**, 1185 (1961).

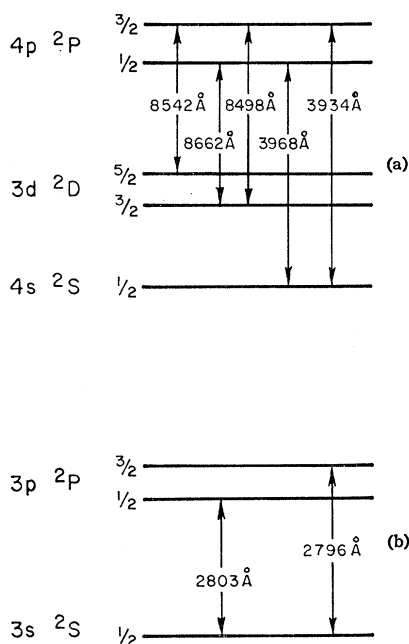


FIG. 1. (a) First few energy levels of Ca^+ .
(b) First few energy levels of Mg^+ .

be treated assuming zero nuclear spin (no hfs) in the Breit formula.

In the experiment we use incident, exit, and magnetic-field axes which are mutually orthogonal, with incident and exit polarizers oriented perpendicular to the field.¹⁵ For this geometry with a $^2S_{1/2}$ ground state and a $^2P_{3/2}$ excited state, the Breit formula predicts a scattered intensity (obtained by evaluating the angular part of the matrix elements in the formula)

$$I(H) = NI_0[1 - cL(x)], \quad (1)$$

where $L(x) = 1/(1+x^2)$ and $x = 4\pi g_J \mu_0 H \tau / h$ (we also use $x = H/\frac{1}{2}H_{1/2}$ following the notation of Wahlquist¹⁶), $I(H)$ is the scattered intensity as a function of magnetic field strength H , I_0 is a normalizing constant, $c=0.6$ for these particular states, N is the number of scatterers, μ_0 is the Bohr magneton, τ is the effective lifetime of the excited state, and we use $g_J = \frac{3}{2}$ for the $^2P_{3/2}$ state.¹⁷ (The difference between this effective lifetime and the natural radiative lifetime is treated in detail in Sec. IVC.) It can be seen that the half-maximum point in the Lorentz lineshape, corresponding to $x=1$ in Eq. (1), occurs at $H \cong \pm 4.3$ G for a typical lifetime of 10^{-8} sec.

In the Ca^+ experiment, an interference filter was used to pass the 3934 and 3968 Å lines (Fig. 1a) while blocking

¹⁵ See Sec. IV E for a discussion of reasons why the geometry is selected.

¹⁶ H. Wahlquist, J. Chem. Phys. 35, 1708 (1961).

¹⁷ For an alkali-like ion, g_J calculated assuming Russell-Saunders coupling should be correct to considerably better than 1%. Even in neutral Hg for example, where there is a significant departure from L - S coupling unlike the alkalis, the measured value of g_J in the 6P_1 state deviates by only 1% from the Russell-Saunders value of 1.5. W. W. Smith, Phys. Rev. 137, A330 (1965).

the remainder of the Ca, Ca^+ , and argon spectrum; in the magnesium experiment, a spectrometer was used to isolate the 2796 and 2803 Å lines (Fig. 1b) from the remaining spectrum, but in both experiments the radiation from the $^2P_{1/2}$ state as well as from the $^2P_{3/2}$ state was detected. At first sight it might be thought necessary to eliminate the ($^2P_{1/2}$ - $^2S_{1/2}$) radiation in order to see a Hanle effect resulting from only the $^2P_{3/2}$ fine structure level, but this is not really necessary, since no Hanle effect can be observed in a $J=\frac{1}{2}$ to $J=\frac{1}{2}$ transition with linearly polarized (or unpolarized) light.¹⁸ Consequently, the $^2P_{1/2}$ - $^2S_{1/2}$ scattering will merely contribute a constant term to Eq. (1), which can be represented by a renormalization and a decrease in the value of c . The finite solid angles actually used in the experiment also decrease the size of the field-dependent term compared to the other term, so that the net result in the experiments was a value $c \cong 0.35$.

In order to obtain the transition probabilities (or oscillator strengths) of each of the transitions from the $\text{Ca}^+ 4^2P_{3/2}$ state (Fig. 1a), one must evaluate the appropriate branching ratios from theory or from a separate experiment. An experiment to obtain these ratios is planned.

III. DESCRIPTION OF THE EXPERIMENT AND APPARATUS

The apparatus used is indicated in Fig. 2. Resonance radiation from a lamp passes through an $f/1.5$ system of lenses and a linear polarizer¹⁹ into the scattering chamber. Light scattered at a mean angle of approximately 90° is collected by a photomultiplier through a second $f/1.5$ lens system, linear polarizer, and interference filter; a magnetic field is applied to the scattering chamber perpendicular to the incident and detected light beams. Some stray light is collected from instru-

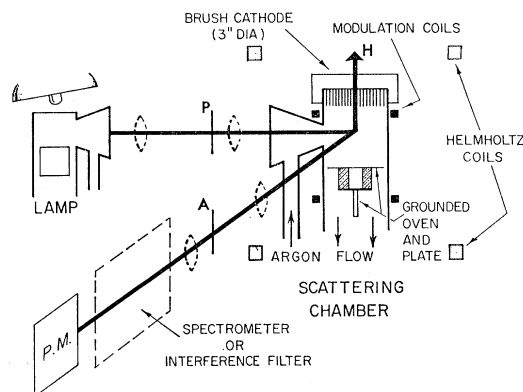


FIG. 2. Schematic diagram of apparatus.

¹⁸ A Hanle effect may be observed in a $J=\frac{1}{2}$ state with circularly polarized light; see A. Gallagher and A. Lurio, Phys. Rev. Letters 10, 25 (1963).

¹⁹ We have used Polacoat coating PL-40 on fused quartz. For its transmission and polarization characteristics see M. N. McDermott and R. Novick, J. Opt. Soc. Am. 51, 1008 (1961).

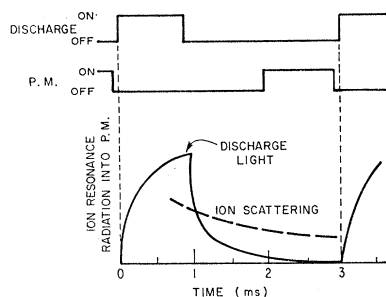


FIG. 3. Typical discharge and photomultiplier timing.

mental scattering as well as from ion resonance radiation originating from the discharge itself. In order to eliminate the bulk of the discharge light and to make it possible to evaluate and eliminate collisional broadening by electrons or by metastable argon atoms produced in the discharge, the discharge is operated on a pulsed basis and the scattering is monitored after turning off the discharge. A typical timing sequence is shown in Fig. 3. The ion population in the scattering region diminishes by half in approximately 5 msec/Torr argon (in the operating region below 1 Torr), while the discharge light dies out much more rapidly than the ion scattering.

The magnetic field in the scattering region is produced by a set of Helmholtz coils with homogeneity of $\sim 0.1\%$ over a 2-in. cube, with a regulated, programmed, dc power supply. Sinusoidal modulation of the magnetic field at 25 cycles/sec with very small harmonic distortion permits the use of lock-in detection of the scattered intensity at either a 25- or a 50-cycle reference frequency. Saturation of the lock-in amplifier at the discharge pulse frequency is prevented by using a low-pass filter, which transmits frequencies 50 cycles/sec and below, at the input to the amplifier. The lock-in signal is plotted as a function of magnet current with an X-Y recorder. The Helmholtz-coil magnetic field was determined as a function of current to an accuracy of 0.1% with the aid of an optically pumped rubidium-vapor magnetometer.²⁰

In the Mg^+ experiment we were not able to obtain an interference filter to separate the MgI resonance line at 2852 \AA from the 2796 \AA MgII resonance line without a considerable sacrifice in peak transmission and high cost. For this reason, we have used an $f/9$ Jarrell-Ash grating spectrometer to isolate the two ion lines from the remaining spectrum. Signal-to-noise ratio is sacrificed compared to the $f/1.5$ system used for Ca^+ , but this did not seriously impair the precision of the measurements.²¹ Because of the lower signal-to-noise in the Mg^+ experiment, many of the checks for systematic error discussed in Sec. IV were carried out only on Ca^+ .

²⁰ See, for example, A. L. Bloom, *Appl. Opt.* **1**, 61 (1962).

²¹ In a different arrangement an interference filter was used in conjunction with an absorption cell which attenuated the MgI resonance line by a factor ~ 100 , but the minor improvement in signal-to-noise ratio did not justify the increased complication.

A. Source of Ion Resonance Radiation

An initial attempt to make a microwave-excited, electrodeless-discharge tube as a source of Ca and Ca^+ resonance radiation was frustrated by the fact that the calcium reacted almost immediately with the quartz walls of the tube when the lamp was brought up to operating temperature. Magnesium electrodeless lamps present similar problems. A small amount of metal in the tube (with a few Torr of argon to sustain the discharge) rapidly cleans up, leaving an argon lamp. A larger quantity of Mg or Ca will discolor the walls so rapidly that no significant amount of light gets out.

Lack of success with the simple electrodeless discharge tube for these reactive metals indicated that a more complex arrangement such as a modification of the Cario-Löchte-Holtgreven flow lamp²² is necessary. Successful flow lamps of this type have been made to work well for both calcium- and magnesium-atom resonance lines by the group at Columbia. Using these lamps with radiofrequency excitation at 15–30 Mc/sec from a 400-W oscillator, we find that the ratio of ion to atom-resonance-line intensities could be made as high as 1:1 with about 15-mW intensity of the 3934 and 3968 Ca^+ lines going into an $f/1.5$ optical system.²³ No attempt was made to purify the tank argon used, and only a mechanical forepump was used to pump out the lamp.

One may speculate that the ion-resonance-line intensity might be increased still further if the electron temperature in the discharge could be increased by the use of microwaves. The result of this consideration was the modified design of the Columbia flow lamps illus-

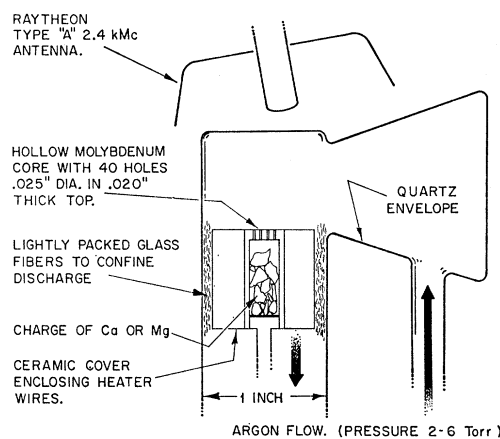


FIG. 4. Microwave-excited flow lamp. The drilled-hole oven top heats well enough to prevent condensing of the Ca or Mg in the passages (a problem encountered with the crinkle-foil plugs described in Ref. 22). The same oven design was used in the scattering chamber, with coaxial heater wires, to minimize their magnetic field.

²² For a review of recent progress in making light sources, see B. Budick, R. Novick, and A. Lurio, *Appl. Opt.* **4**, 229 (1965).

²³ Our ~ 15 -mW output figure agrees with the 16-mW maximum output given in Ref. 22, assuming an $f/1.5$ optical system (the actual aperture used is not stated in Ref. 22, however, and we were driving the lamp with considerably more rf power).

trated in Fig. 4. Merely by using microwave excitation, and without further optimization of the geometry or the use of a cavity²⁴ to enclose the lamp, we obtain roughly four times the output intensity in the 3934–68 Å ion lines and in the 4227 Å atom resonance line that we had with the original flow-lamp design in Ref. 22. The microwave power output of the magnetron is approximately 100 W, of which only a small fraction actually excites the discharge; no upper limit on the amount of ion resonance radiation was reached with the power available.

B. Source of Ions

A dilute vapor of Group II metal ions was produced in both rf and dc discharge scattering chambers (the latter is shown in Fig. 2). The scattering chamber designed for rf excitation at 15–30 Mc/sec was similar to that in Fig. 2, but had a quartz cover where the brush cathode is shown. The oven sprayed an atomic beam of calcium (or magnesium) up into the scattering region. The two side windows for the incident and scattered beams of resonance radiation were protected from becoming coated with calcium (magnesium) by an argon flow (as indicated). An rf discharge between the grounded oven and an electrode painted on the glass above produced a plasma of argon and calcium (magnesium) in the scattering region above the oven. By varying the rf power or the oven temperature, the density of Ca⁺ (Mg⁺) ions was controlled.

Figure 2 shows the scattering chamber in which a “brush cathode” dc discharge produced the ions. This type of cold-cathode discharge, designed by Persson of the National Bureau of Standards,²⁵ produces a relatively stable plasma in a large volume by means of a “beam” of high-energy electrons. The temperature of the vast majority of electrons not in the main beam is quite low, corresponding to ~0.05–0.10 eV. Calcium (magnesium) vapor from the oven is sprayed up into the observation region containing argon (again a continuous flow) several centimeters from the cathode. At argon pressures of 0.1 to ~1.0 Torr, one can produce a sufficient number of Ca⁺ (Mg⁺) ions in the observation region to give multiple scattering of the resonance radiation with only a slow plating of metal on the container walls. Typical operating conditions for the brush cathode were 0.3 Torr argon, 300–500 V dc on cathode, and 50 mA instantaneous discharge current. The brush discharge produced less ion resonance radiation than the rf discharge, and also appeared to have a slight advantage in stability. All data reported for Ca⁺ and Mg⁺ were taken with the brush cathode discharge.

IV. DETAILS OF THE EXPERIMENT

A. Field Dependence of the Discharge

A new complication which arises in these ion Hanle-effect experiments, as contrasted with atom Hanle-

effect experiments, is that the ions are produced in a plasma which interacts with the applied magnetic field. As a result, the ion density N in Eq. (1) becomes a slowly varying function of the magnetic field, and the Hanle-effect and ion-density field dependences must be unscrambled. We have done this by detecting the ion resonance fluorescence first with both polarizers oriented parallel to the applied magnetic field (which gives no Hanle effect), then with both polarizers oriented perpendicular to the field. In this way we can measure first a signal proportional to $N(H)$ and then to $N(H) \times [1 - cL(H)]$ for the same optically illuminated region under identical discharge conditions, and the $N(H) \times [1 - cL(H)]$ signal can be corrected for the field dependence of $N(H)$ so that $L(H)$ can be obtained.

Over the entire argon-pressure range and scattering-ion-density range reported in the experiments, $N(H)$ varied slowly enough with field strength to produce less than 5% difference between the apparent width of the uncorrected signal, $N(H)[1 - cL(H)]$, and the width of $L(H)$. Since the discharge conditions varied greatly with argon and calcium (or magnesium) pressures and with the discharge current, the sign and magnitude of the width correction varied in a fairly random fashion throughout the data. Thus we have concluded that any residual inaccuracy introduced by the variation in $N(H)$ appears as part of the scatter in the data (Figs. 6 and 7) but does not produce any systematic error.

B. Modulation Detection

Small-amplitude field modulation and lock-in detection at the modulation frequency results in a lock-in output, after $N(H)$ corrections, which closely approximates the derivative of the Lorentzian shaped $L(H)$. The exact expression for this signal has been calculated using Fourier integrals by Wahlquist¹⁶ (it is identical to his a_1 amplitude). The Hanle-effect linewidth can be determined from this signal by sweeping the field between approximately $\pm \frac{1}{2}H_{1/2}$, correcting for the variation of $N(H)$, then measuring the peak-to-peak separation, and correcting for modulation broadening. Since finding the peak positions from such data is a tedious process, and since the peak positions measured in this manner are strongly influenced by intensity drifts during the sweep time of the dc field, we have measured the widths by driving the lock-in reference with the first harmonic of the modulation frequency, so that the lock-in [output after the $N(H)$ correction] has the shape of Wahlquist's a_2 amplitude. For small amplitude modulation, with amplitude H_ω , a_2 closely approximates the second derivative of $L(H)$, with zeros occurring at $H = \pm \frac{1}{6}\sqrt{3}H_{1/2}(1 + \frac{1}{2}H_\omega^2/(\frac{1}{2}H_{1/2})^2)$. The positions of these zeros were measured by sweeping the field over a small region centered on each zero as many times as necessary to obtain sufficient accuracy. Aside from the $N(H)$ correction, which produced the equivalent of a slight zero offset, this null detection method was independent of even large amplitude drifts; in addition,

²⁴ See M. Zelickoff *et al.*, J. Opt. Soc. Am. 42, 818 (1952).

²⁵ K. B. Persson, Natl. Bur. Std. (U. S.) Rept. 8452 (1964); Bull. Am. Phys. Soc. 10, 191 (1965).

all of the signal integration time was applied to finding the zeroes of $I''(H)$. For simplicity, the $N(H)$ correction was applied by assuming the lock-in output could be represented by $I''(H)$ rather than the second Fourier amplitude of $I(H+H_\omega \sin \omega t)$ as in Ref. 16. The resulting inaccuracies in this correction were maintained at less than 1% of the linewidth by operating at

$$H_\omega / \frac{1}{2} H_{1/2} \approx \frac{1}{3}.$$

As a check on the validity of this method of measuring linewidths, several Ca⁺ linewidths, measured under various discharge conditions in the range of a few percent multiple-scattering narrowing and a few percent collisional broadening, were compared to those measured by lock-in detection at the reference frequency and by dc detection [with $N(H)$ corrections in all cases]. After corrections for modulation broadening, the results all agreed within the 1–2% scatter of the dc widths.

As an additional check on the validity of the results, lock-in signals were compared, after $N(H)$ corrections, to Wahlquist's a_1 and a_2 coefficients, with the resulting agreement shown in Fig. 5. The dc signal profiles were also compared to a Lorentzian shape; the results are presented in Sec. IVD where they were also used to investigate the lamp line profile.

C. Multiple-Scattering Narrowing and Collisional Broadening

The linewidth of the Lorentzian-shaped intensity resonance of the Hanle effect corresponds to an effective lifetime τ_{eff} of the excited state. This effective lifetime can differ from the natural lifetime of the excited state as a result of multiple scattering of photons⁵ and collisions with other gases.^{26–28} The additivity of these effects has been fairly well verified in double-resonance experiments under conditions of much greater multiple-scattering narrowing and collisional broadening than occurred in our experiments.²⁶ Consequently, we have assumed such an additivity for our Hanle-effect linewidths:

$$4\pi g \mu_0 (\frac{1}{2} H_{1/2}) / h \cong 1 / \tau_{\text{eff}} = (1 - \alpha x) / \tau + n \bar{v}_{12} \sigma, \quad (2)$$

where n is the density of broadening gas atoms,

$$\bar{v}_{12} = \left[\frac{8}{\pi} RT \left(\frac{1}{M_1} + \frac{1}{M_2} \right) \right]^{1/2}$$

is the mean relative velocity of the colliding ions and particles, σ is the "alignment" depolarization cross section for collisions with argon,²⁹ τ is the natural lifetime

²⁶ F. W. Byron and H. M. Foley, Phys. Rev. **134**, A625 (1964).

²⁷ A. Omont, J. Phys. Radium **26**, 26 (1965).

²⁸ M. I. D'Yakonov and V. I. Perel, Zh. Eksperim. i Teor. Fiz. **48**, 345 (1965) [English transl.: Soviet Phys.—JETP **21**, 227 (1965)].

²⁹ This conventional definition of the cross section is adopted in Refs. 26–28. In Refs. 27 and 28 the relationship between "orientation" and "alignment" depolarization cross sections is derived. It has also been experimentally verified: W. Happer and E. B. Saloman, Phys. Rev. Letters **15**, 441 (1965).

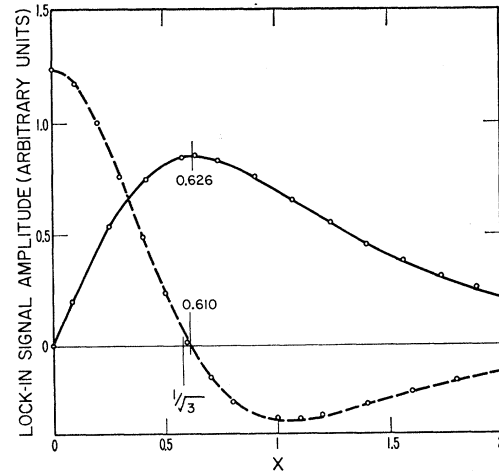


Fig. 5. Experimental versus theoretical lock-in signals from the Ca⁺ experiment. Solid line is lock-in signal with reference frequency equal to modulation frequency; dashed line at twice the modulation frequency. Circles are Wahlquist a_1 and a_2 coefficients with $\beta \cong \frac{1}{2} H_{1/2} / H_\omega = 3$. The vertical scales and horizontal scale of the experimental curves are chosen to fit at the peaks and zero; β is known from the measured modulation broadening.

time of the $^2P_{3/2}$ state, $x = 1 - \exp(-kN)$, N is the ion density, and α and k are coefficients which depend on the states involved (the formulas for α and k can be found in Ref. 5 or 26, $\alpha = 0.35$ in this case).

In our experiments in which the multiple-scattering narrowing was maintained at less than 10% of the natural linewidth, x varies almost linearly with N ; and Eq. (2) takes on the form used to interpret the experiments:

$$4\pi g \mu_0 (\frac{1}{2} H_{1/2}) / h \cong (1 - \alpha k N) / \tau + n \bar{v}_{12} \sigma. \quad (3)$$

The scattering-chamber discharge produces a considerable number of argon metastable atoms and free electrons, and it might be expected that these could contribute to the collisional broadening of the Hanle-effect linewidths. This possibility was investigated by measuring the Ca⁺ linewidths during the discharge and during different intervals after the discharge was turned off. Under typical conditions the Ca⁺ linewidth was broadened several percent while the discharge was on. At all argon pressures below 1 Torr the broadening diminished to less than 1% by 0.5 msec after the discharge was off, and no further changes were found between 1 and 5 msec after the discharge was turned off (after corrections were made for the decreasing multiple scattering narrowing with decreasing number of ions later in the afterglow). Consequently, the majority of the Ca⁺ and Mg⁺ data was taken by detecting the scattering 1–2 msec after the discharge was turned off.

Once the collisional broadening by discharge products had been eliminated, the measured linewidths were expected to be in accordance with Eq. (3), where n is the density of argon atoms. Consequently the number of calcium (or magnesium) ions in the scattering chamber was varied at a number of argon pressures to

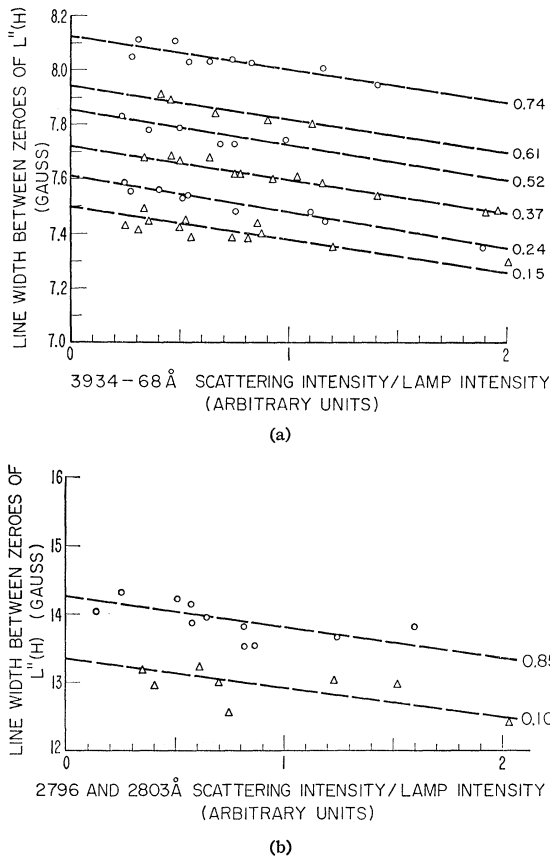


FIG. 6. Hanle-effect linewidth ($H_{1/2}/\sqrt{3}$) versus relative ion density at a number of argon pressures (in Torr). Widths have been corrected for the $\sim 6\%$ modulation broadening. (a) Ca^+ data. (b) Mg^+ data: the scatter here is much greater than for the Ca^+ data due to intensity lost using a spectrometer. To avoid mingling, data at only two pressures are presented.

establish the $N=0$ limit of Eq. (3) for each argon pressure (Fig. 6); then these limiting widths were plotted against the argon pressure (Fig. 7) to establish the $N=0$ and $n=0$ limit (i.e., the natural lifetime). Since only the relative number of ions is needed in order to establish the $N=0$ limits in Fig. 6, and since the optical depth for the ion resonance radiation is much less than 1, the intensity of scattered resonance radiation was used as the index of the scattering ion density.

The ion density was varied by changing the oven temperature, and by changing the discharge current. The former method has the advantage of establishing the limit of zero $\text{Ca}(\text{Mg})$ ion density and zero $\text{Ca}(\text{Mg})$ atom density at the same time so that any collisional broadening by Ca or Mg , although not expected to be significant at the experimental densities of less than 10^{-2} Torr, will not influence the limiting widths. Changing the discharge current was used to verify that the discharge intensity did not influence the linewidths through some mechanism such as heating the argon to change its density at fixed pressure, or producing more

electrons. The linear dependence of the widths on N and n , as predicted by Eq. (3), is consistent with the results in Figs. 6 and 7 and is at the same time a considerable aid in finding the limiting widths.

D. Influence of Lamp Profile

The Breit formula is valid when the power density of the lamp radiation is constant across the Doppler-shaped absorption band of the scattering ions. The effect of a divergence from a flat exciting spectrum can be exactly evaluated in terms of the power density,³⁰ but its major features can be considered as arising from the magnetic scanning of the lamp line profile by the absorption profile of the scatterers. For the Hanle-effect linewidths and the lamp Doppler widths of the present experiments, this scanning effect should produce less than 1% error in the lifetimes if the lamp is not badly self-reversed, and little self-reversal is expected for our lamp design. This expectation was tested for Ca^+ in two ways: by looking for changes in the Hanle-effect linewidths while varying the power level and oven temperature of the lamp, and by comparing the field dependence of the scattering intensity to a Lorentzian shape.

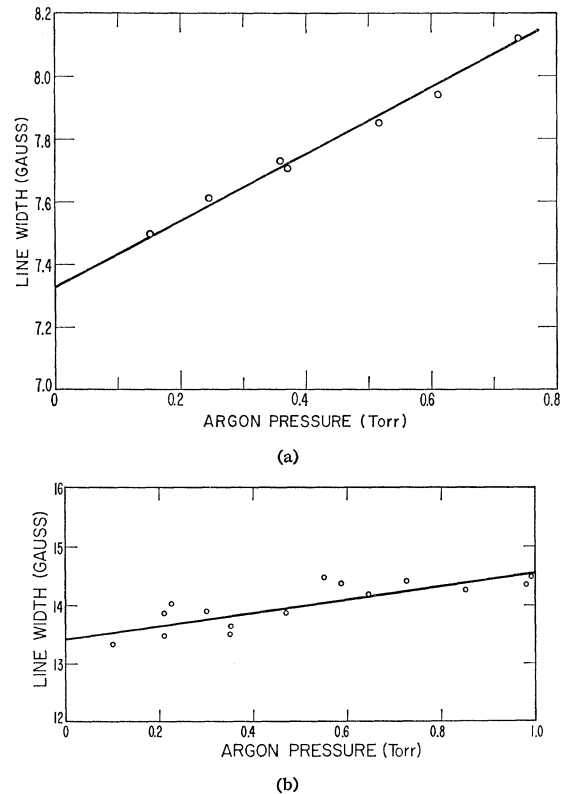


FIG. 7. Extrapolated zero-ion-density linewidths versus argon pressure. (a) Ca^+ width from Fig. 6(a). (b) Mg^+ widths from Fig. 6(b) and additional data. Typically five widths were measured to establish each point in Fig. 7(b).

³⁰ A. Gallagher and A. Lurio, Phys. Rev. **136**, A87 (1964).

The linewidths measured with altered lamp conditions changed less than 1% as the lamp power and calcium density were each varied by a factor of 3, supporting the expectation of a sufficiently flat lamp line profile.

The possibility of a divergence from Lorentzian field dependence was investigated by the following method. $I(H)$ was measured with H varying between $\pm 2.5H_{1/2}$ and was corrected for the slight $N(H)$ variation; then any asymmetry was removed by averaging the positive and negative field results (causes of asymmetry are discussed in Sec. IVE). For our scattering geometry, any lamp profile effects should be symmetric in field and should thus produce the approximate effect of multiplying the scattering intensity in Eq. (1) by $1 + \alpha H^2 / (\frac{1}{2}H_{1/2})^2$ with $|\alpha| \ll 1$. Labeling the experimentally measured $I(H) - I(0)$ as S , it then follows that

$$\frac{S}{H^2} \cong \frac{1}{(\frac{1}{2}H_{1/2})^2} \left\{ cI_0N - S + \alpha I_0N \left[1 - c + \frac{S}{cI_0N - S} \right] \right\},$$

where only first-order terms in α have been kept. Thus for $\alpha = 0$, a plot of S/H^2 versus S will be a straight line of slope $-(\frac{1}{2}H_{1/2})^{-2}$, with S varying from 0 at $H=0$ to cI_0N at $H=\infty$. If α is not zero, the divergence of the data from a straight line will become apparent as S approaches cI_0N [at the maximum fields used, $S/(cI_0N - S) \cong 20$]. The advantages of plotting the data in this manner are that the values of neither cI_0N nor $\frac{1}{2}H_{1/2}$ need be assumed, and the variation in $\frac{1}{2}H_{1/2}$ due to a lack of Lorentzian shape appears as the variation in the slope of the line. Ca⁺ data taken at several different scattering chamber conditions in the range of a few percent multiple-scattering narrowing and collisional broadening are presented in Fig. 8. The close fit to straight lines would appear to verify the validity of the $N(H)$ corrections as well as of the flatness of the lamp line profiles.

E. Deviations from Perfect Scattering Angles

The intensity of resonance fluorescence for arbitrary incident and exit angles and polarizer orientations can be calculated from the Breit formula by evaluating the angular dependence of the matrix elements for our $^2S_{1/2}$ ground state and $^2P_{3/2}$ excited state ($I=0$) case. The result is

$$I(H) = NI_0 \left\{ 0.8 + 0.2(3e_z^2 - 1)(3e_z'^2 - 1) + 0.6 \frac{\text{Re}(e_+^2 e_-'^2)}{1+x^2} \right. \\ \left. + 0.6 \frac{x \text{Im}(e_+^2 e_-'^2)}{1+x^2} + 2.4e_z e_z' \frac{\text{Re}(e_+ e_-')}{1+(x/2)^2} \right. \\ \left. + 2.4e_z e_z' \frac{(x/2) \text{Im}(e_+ e_-')}{1+(x/2)^2} \right\}, \quad (4)$$

where e_{\pm} , e_z , e_{\pm}' , and e_z' are defined as in Ref. 3. As noted

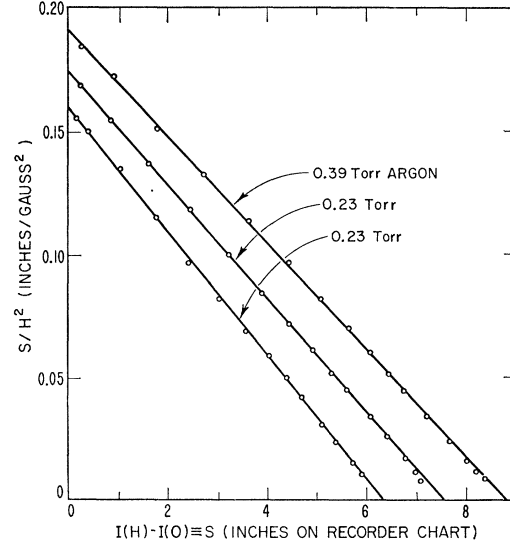


FIG. 8. $I(H)$ data from the Ca⁺ experiment. The two upper line-shapes were measured at a Ca⁺ density that produced approximately 1% multiple-scattering narrowing, while the lower line-shape was taken with approximately 3% multiple-scattering narrowing.

in Sec. II, $I(H)$ becomes $NI_0[1 - 0.6/(1+x^2)]$ in the case of 90° scattering in the plane perpendicular to the field with polarizers oriented perpendicular to the field.

Small differences between these ideal angles and the average scattering angles of the experiments can easily arise in a wide-angle optical system, thereby causing the last three terms of Eq. (4) to contribute to the signal. The first of these terms can appear if there is an error in the average scattering angle, $\langle \phi - \phi' \rangle_{av}$, whereas the last two terms will contribute only in proportion to $\sin \delta \sin \delta'$ where δ and δ' are, respectively, the errors in the in and out polarizer angles. Consequently, it is primarily the $x/(1+x^2)$ term which produces an asymmetry in the signal with the amount of asymmetry depending on $\langle \phi - \phi' \rangle_{av}$. Because the change in symmetry is first order in the amplitude of this term, but the measured linewidth changes only to second order in the amplitude, this source of width error is easily controlled. In these experiments we measured the maxima P_+ and minima P_- of $I'(H)$ with the lock-in detector and adjusted $\langle \phi - \phi' \rangle_{av}$ until $P \equiv (P_+ - P_-)/(P_+ + P_-)$ was less than 0.1. Under these conditions the fractional change in width, which we calculate to be $4P^2/9$, was less than 0.5%.

We must also consider the possibility that the polarizer angles are sufficiently in error to produce significant contributions from the last two terms in Eq. (4) (e.g., a small component of transverse field can change the dc field direction). In this case the change in measured linewidth due to the last (asymmetric) term will be second order in its amplitude and quite negligible. The symmetric term will broaden the linewidth by first order in its amplitude, but the largest contribution to

this amplitude is proportional to $\sin\delta \sin\delta' \sin\langle\Delta\phi\rangle_{av}$, where $\langle\Delta\phi\rangle_{av}$ is the error in $\langle\phi-\phi'\rangle_{av}$. Consequently this amplitude will also be quite negligible when $\langle\phi-\phi'\rangle_{av}$ is adjusted to produce a fairly symmetric signal.

These conclusions were tested in the Ca^+ experiment by varying the polarizer angles several degrees and also by removing the input beam polarizer; less than 1% width change resulted.

F. Atomic Lifetimes

The neutral calcium 4^1P_1 lifetime and magnesium 3^1P_1 lifetime have already been accurately measured by the Hanle-effect technique^{3,31} and by the phase-shift technique.³² Nonetheless, it appeared desirable to measure them in our apparatus, since we would obtain a general check on our apparatus and at the same time would obtain the argon collisional depolarization cross sections for these states.

Line-profile investigation on these atomic lines following the methods in Sec. IVD, led to the same results found for the ion lines: that the lamp line profile was sufficiently flat to produce less than 1% error in the lifetimes.

The influence of a several percent multiple-scattering narrowing and collisional broadening were found to be consistent with Eq. (3) (with N representing the atomic density).

Our results for the $\text{Ca } 4^1P_1$ and $\text{Mg } 3^1P_1$ lifetimes are

$$\tau(\text{Ca } 4^1P_1 \text{ state}) = (4.62 \pm 0.15) \times 10^{-9} \text{ sec}$$

and

$$\tau(\text{Mg } 3^1P_1 \text{ state}) = (2.03 \pm 0.06) \times 10^{-9} \text{ sec.}$$

These are in satisfactory agreement with previous lifetime results, which are

$$\tau(\text{Ca } 4^1P_1 \text{ state}) = (4.48 \pm 0.15) \times 10^{-9} \text{ sec from Ref. 3,}$$

$$\tau(\text{Mg } 3^1P_1 \text{ state}) = (1.99 \pm 0.08) \times 10^{-9} \text{ sec from Ref. 31,}$$

and

$$\tau(\text{Ca } 4^1P_1 \text{ state}) = (4.67 \pm 0.11) \times 10^{-9} \text{ sec from Ref. 32.}$$

V. CONCLUSIONS

From the best-fit lines in Figs. 7a and 7b, and from an estimate of possible systematic errors, we obtain

$$\tau(\text{Ca}^+ 4^2P_{3/2} \text{ state}) = (6.72 \pm 0.20) \times 10^{-9} \text{ sec,}$$

and

$$\tau(\text{Mg}^+ 3^2P_{3/2} \text{ state}) = (3.67 \pm 0.18) \times 10^{-9} \text{ sec.}$$

The uncertainty in the Mg^+ lifetime is considered to be greater than that for Ca^+ because most of the tests for systematic error were performed only with Ca^+ . Since the same methods and apparatus were used in the Mg^+ experiment, it appears likely that these systematic

errors were also absent in the Mg^+ data; but this was not proven owing to the low intensities available when using a spectrometer.

The $\text{Ca}^+ 4^2P_{3/2}$ state lifetime cannot be compared directly to the theoretical predictions for the $4^2P_{3/2} - 4^2S_{1/2}$ oscillator strength,¹ since the $4^2P_{3/2}$ state decays by three transitions. Since we plan to measure the branching ratios for these three transitions, we will not try here to establish their most likely values from available approximate values.

Our $\text{Mg}^+ 3^2P_{3/2}$ state lifetime is compared in Table I (see Refs. 33–35) to all the other experimental and theoretical results that we are aware of.

The slopes of the best fit lines in Fig. 7, and the equivalent data for the neutral calcium and magnesium 1P_1 states, can be used to establish the collisional depolarization cross sections defined in Eq. (2). It is also necessary to establish the average temperature of the vapor in the scattering region, since $n\bar{v}_{12}$ is proportional to $T^{-1/2}$ at any particular argon pressure and σ is expected to vary as $T^{-1/5}$. The vapor in the scattering region above the oven is heated by the oven in competition with cooling by the walls of the scattering chamber and by circulation of the argon. The mean free path of calcium (magnesium) in 0.1–1 Torr argon is such that it will be in thermal equilibrium with the argon by the time it reaches the optically illuminated region 3–17 mm above the oven; also, measurements of Ca^+ linewidths versus the discharge current showed no dependence on the current, indicating that the discharge did not significantly heat the vapor. Consequently, the temperature profile of the vapor in the scattering region was measured with a thermocouple probe while the discharge was off and the oven was at its typical temperature. The measured temperatures varied only slightly with argon pressure, but varied from 210°C at 3 mm above the oven to 120°C at 10 mm, and 80°C at 17 mm. We have used $140 \pm 50^\circ\text{C}$ to calculate $n\bar{v}_{12}$. The resulting alignment depolarization cross sections at 140°C for collisions with argon are

$$\sigma(\text{Mg } 3^1P_1 \text{ state}) = (1.9 \pm 0.3) \times 10^{-14} \text{ cm}^2$$

$$\sigma(\text{Mg}^+ 3^2P_{3/2} \text{ state}) = (1.3 \pm 0.25) \times 10^{-14} \text{ cm}^2$$

$$\sigma(\text{Ca } 4^1P_1 \text{ state}) = (1.9 \pm 0.3) \times 10^{-14} \text{ cm}^2$$

$$\sigma(\text{Ca}^+ 4^2P_{3/2} \text{ state}) = (1.4 \pm 0.2) \times 10^{-14} \text{ cm}^2.$$

The theory of collisional depolarization of excited atomic states in atom-atom collisions has been developed in Refs. 26, 27, and 28 and applied to Hg, Cd, and Zn collisions with similar atoms and foreign gas atoms. In the case of ion-atom collisions, which are of course nonresonant, the excess charge q of the ion adds a term $q\mathbf{P} \cdot \mathbf{R}R^{-3}$ to the $3(\mathbf{P} \cdot \mathbf{R})(\mathbf{R} \cdot \mathbf{R})R^{-5} - \mathbf{P} \cdot \mathbf{R}R^{-3}$ (dipole-

³³ L. Biermann and K. Lübeck, *Z. Astrophys.* **25**, 325 (1948).

³⁴ D. R. Bates and A. Damgaard, *Proc. Roy. Soc. (London)* **A242**, 101 (1949).

³⁵ C. H. Corliss and W. R. Bozman, *Natl. Bur. Std. (U. S.) Monograph* **53**, (1962). Note discussion of accuracy, p. XV.

³¹ A. Lurio, *Phys. Rev.* **136**, A376 (1964).

³² E. Hulpke, E. Paul, and W. Paul, *Z. Physik* **177**, 257 (1964).

TABLE I. Lifetime of $\text{Mg}^+ 3^2P_{3/2}$ state.

Method	Reference	Result
SCF ^a with exchange and polarization approximations	33	3.84×10^{-9} sec
Coulomb approximation	34	3.97×10^{-9} sec
Arc emission	35	4.4×10^{-9} sec
Hanle effect	present work	$(3.67 \pm 0.18) \times 10^{-9}$ sec (std. dev. of $\log_{10} \tau = 0.27$)

^a Self-consistent-field.

dipole) perturbation potential of atom-atom collisions. (\mathbf{P} is the dipole operator for the atom, $\mathbf{\Pi}$ is the dipole operator for the ion, and \mathbf{R} is the internuclear vector.) It can be seen that this additional term will not directly produce changes in the density matrix of an excited state of the ion. The added term does make a contribution ($\sim R^{-6}$) in second-order perturbation theory when it is multiplied by a matrix element involving the

electron quadrupole operator for the ion and the electron dipole operator for the atom. Second order is also the lowest order in which the dipole-dipole perturbation contributes (again $\sim R^{-6}$). One can verify that the added term involves matrix elements and energy denominators of the same order of magnitude as the dipole-dipole term. For this reason it is not surprising that the Group II ion-argon and atom-argon depolarization cross sections are of the same order of magnitude; they are also comparable to the theoretical and experimental cross sections for argon collisions with Hg in the lowest 3^1P_1 state quoted in Table II of Ref. 26.

ACKNOWLEDGMENTS

We wish to thank L. Branscomb for suggesting the measurements of ion-excited-state lifetimes, P. Bender for his helpful discussions, and R. Weppner for his assistance in building the apparatus.

Calculation of Auto-Ionization Rates*

STEVEN TRENT MANSON

Physics Department, Columbia University, New York, New York

(Received 21 December 1965)

A method has been formulated to calculate auto-ionization rates by perturbation theory with no internal inconsistencies. Calculations have been carried out in $(2s)^2 1S$ He, $(2s, 2p) 1^3P$ He, $(1s, 2s, 2p) 4P_{5/2}$ Li, and $(1s, 2s, 2p) 2P_{\pm}$ Li. The applicability of this formulation, as well as how it differs from previous perturbation methods, is discussed.

I. INTRODUCTION

AN atom in an excited state lying above the first ionization potential may undergo a radiationless decay into the continuum. This is the phenomenon of auto-ionization. It is of significance in the interpretation of atomic spectra as well as being one of the more important processes in the upper atmosphere.

Many attempts¹⁻⁶ have been made to calculate the decay rate of auto-ionizing states. We shall be concerned with the perturbation-theory approach in this paper. A

formulation is here presented which removes the internal inconsistencies that occurred in previous perturbation-theory calculations and is then used to calculate auto-ionization decay rate in certain states of helium and lithium.

Throughout this paper atomic units are used unless otherwise specified, i.e., $\hbar = e = m_{\text{electron}} = 1$.

II. THE GOLDEN RULE

Suppose we have an atom with Hamiltonian H , and that at $t=0$ the atom is known to be in a state $|\varphi\rangle$. Let H_0 be a Hamiltonian such that

$$H_0|\varphi\rangle = E_0|\varphi\rangle, \quad (1)$$

where E_0 is the energy of the state. In the Schrödinger representation, then, $|\psi_s(t=0)\rangle = |\varphi\rangle$. Now we transform to the interaction representation defined by H_0 ; $|\psi_{\text{int}}(t=0)\rangle = |\varphi\rangle$. Define

$$H_1 = H - H_0. \quad (2)$$

* This work was supported in part by the U. S. Atomic Energy Commission and in part by the National Science Foundation.

¹ Ta-You Wu, *Phys. Rev.* **66**, 291 (1944).

² J. Cooper, in *Atomic Collision Processes* (North-Holland Publishing Company, Amsterdam, 1964), p. 595.

³ R. Kh. Propin, *Opt. i Spetroskopiya* **8**, 300 (1960) [English transl.: *Opt. Spectry.* (USSR) **8**, 158 (1960)].

⁴ R. Kh. Propin, *Opt. i Spetroskopiya* **10**, 289 (1961) [English transl.: *Opt. Spectry.* (USSR) **10**, 155 (1961)].

⁵ B. Bransden and A. Dalgarno, *Proc. Phys. Soc. (London)* **A66**, 904 (1953).

⁶ P. G. Burke, D. D. McVicar, and K. Smith, *Phys. Rev. Letters* **11**, 559 (1963).